

Research on Engineering Structures & Materials



www.jresm.org



Development and validation of an accurate analytical solution for hoop stress distribution in cylindrical functionally graded materials

Jamiatul Akmal, Adam Wisnu Murti, Asnawi Lubis, Masdar Helmi

Online Publication Date: 30 May 2025

URL: http://www.jresm.org/archive/resm2025-777an0324rs.html

DOI: http://dx.doi.org/10.17515/resm2025-777an0324rs

Journal Abbreviation: Res. Ena. Struct. Mater.

To cite this article

Akmal J, Murti A W, Lubis, Helmi M. Development and validation of an accurate analytical solution for hoop stress distribution in cylindrical functionally graded materials. *Res. Eng. Struct. Mater.*, 2025; 11(5): 2521-2535.

Disclaimer

All the opinions and statements expressed in the papers are on the responsibility of author(s) and are not to be regarded as those of the journal of Research on Engineering Structures and Materials (RESM) organization or related parties. The publishers make no warranty, explicit or implied, or make any representation with respect to the contents of any article will be complete or accurate or up to date. The accuracy of any instructions, equations, or other information should be independently verified. The publisher and related parties shall not be liable for any loss, actions, claims, proceedings, demand or costs or damages whatsoever or howsoever caused arising directly or indirectly in connection with use of the information given in the journal or related means.



Published articles are freely available to users under the terms of Creative Commons Attribution - NonCommercial 4.0 International Public License, as currently displayed at here (the "CC BY - NC").



Research on Engineering Structures & Materials



www.jresm.org

Research Article

Development and validation of an accurate analytical solution for hoop stress distribution in cylindrical functionally graded materials

Jamiatul Akmal *,1,a, Adam Wisnu Murti 2,b, Asnawi Lubis 1,c, Masdar Helmi 3,d

- ¹Dept. of Mechanical Eng., Universitas Lampung, Bandar Lampung 35145, Indonesia
- ²Dept. of Agricultural Technology, Politeknik Negeri Lampung, Bandar Lampung 35141, Indonesia
- ³Dept. of Civil Eng., Universitas Lampung, Bandar Lampung 35145, Indonesia

Article Info

Abstract

Article History:

Received 24 Mar 2025 Accepted 29 May 2025

Keywords:

Cylindrical FGM; Analytical solution; Stress distribution Functionally graded materials (FGMs) are a type of composite material whose microstructure is not homogeneous, differing at each coordinate position. The development of FGM material technology is an important and strategic effort to meet the needs of an increasingly advanced industry. Theoretically, an important topic that is commonly discussed for mechanical applications is the analytical solution of stress distribution in FGM materials subjected to mechanical loads. Previous studies have proposed a stress distribution solution in cylindrical FGM, but the solution is inaccurate in certain applications. Other studies propose stress distribution solutions, but with different boundary conditions. The present study proposes a new solution different from previous studies and valid for applying to cylindrical FGMs with more general inhomogeneity. The developed solution uses a power function to determine the inhomogeneity constant and applies internal pressure under axisymmetric conditions. The solution proposed in this study was validated through numerical simulations (FEM), and a good agreement is obtained with an error value of less than 2.77%. Moreover, the proposed solution shows good agreement with experimental data from previous studies.

© 2025 MIM Research Group. All rights reserved.

1. Introduction

One of the problems in industrial applications is the difficulty of obtaining products from a homogeneous material that meets all property requirements. For example, it isn't easy to produce pipes that are strong, corrosion-resistant, and heat-resistant at the same time using a homogeneous material. These properties can be obtained by combining the advantages of several different materials into a composite material. Such composite materials can be categorized as functionally graded materials (FGMs), whose microstructure differs at each coordinate position with a specific gradient. Different properties include Young's modulus, shear modulus, and density [1], [2]. FGM materials can be categorized as continuous degradation and layered degradation [3]. Examples of continuous degradation of FGM are bamboo [4] and bone [5], while examples of step degradation FGM are layered composite cylinders [6], [7]. With FGM technology, advantages can be obtained, for example, to reduce the intensity factor on the plane and lateral tensions, to obtain a more even distribution of tension, and to improve thermal performance [8], [9].

The development of FGM material technology includes various fields of study, such as raw materials, production processes, mechanical property analysis, and design methods [3]. FGM materials have been used in various fields of application, for example, in the construction of deep

*Corresponding author: jamiatul.akmal@eng.unila.ac.id

^aorcid.org/0000-0002-5915-7681; ^borcid.org/0009-0008-9521-9051; ^corcid.org/0009-0004-7447-5145;

dorcid.org/0000-0001-6781-8948

DOI: http://dx.doi.org/10.17515/resm2025-777an0324rs

Res. Eng. Struct. Mat. Vol. 11 Iss. 5 (2025) 2521-2535

offshore oil and gas operations [10, 11], high-pressure vessels [12, 13], heat-resistant and corrosion-resistant pipes for geothermal power plants [14, 15], and reactor tubes in nuclear structures [16]. For the future, it is predicted that FGM materials will be increasingly needed due to technological advances in various industrial fields, but in this article, the discussion is limited to cylindrical structure FGM. Examples of previous studies include the static analysis of FGM cylindrical shells and the effects of stress concentration [17, 18], the vibration and stability of FGM cylindrical shells subjected to external pressures [19, 20], and the nonstationary response of stepped composite cylindrical shells with drop-off plies under moving random loads [21]. Recently, FGM laminated composite cylinders have been researched for the construction of submerged floating tunnel bridges (SFT-Bridges), which require strong, ductile, and corrosion-resistant structures [22-24].

Cylindrical FGM is commonly used in the industrial sector, for example, for pipes and pressure vessels. The properties of the modulus of elasticity are modeled as exponential equations, where the exponent is the degree of inhomogeneity (β). With an exponential equation, the value of the modulus of elasticity can be determined at each coordinate position. The value of the modulus of elasticity is assumed to vary as $E(r) = E_0 r^\beta$ along the wall thickness. E_0 is the stiffness on the outermost surface (r=1), and β is the empirically determined inhomogeneity constant. An important theme discussed in this study is the equation of stress distribution at each point along the radial axis. Previously, the exact solution had been published by [25], who used mathematical methods to obtain an exact solution for stress distribution in cylinders. The solution was developed from a boundary condition where there was only internal pressure on the inner surface of the cylinder. The article [25] presents the results of radial stress distribution and circumferential stress distribution, as well as the influence of variations in the modulus of elasticity of materials on the distribution of stress.

The problem is that the hoop stress equation proposed by [25] is only valid for β =1, but not for other β values. In addition, the article does not explain in detail the process of developing the equation, making it difficult to understand. Twenty years later, [26] made a new proposal for a stress distribution analytical solution in cylindrical FGM. However, this proposal does not precisely address the existing problems because the solutions developed are based on different boundary conditions. The boundary conditions include: (first) internal pressure applied on the inner surface and tension applied on the outer surface; (second) fixed displacement applied on the inner surface and tension on the outer surface; and (third) internal pressure applied on the inner surface and fixed displacement on the outer surface. Nevertheless, the research in [26] provides a more detailed explanation of the equation development process, making it easier to follow.

This study proposes a new equation for the distribution of hoop stress in cylindrical FGMs with varying inhomogeneity constants (-2 < β < 2). The solution is developed from the boundary conditions: internal pressure is applied on the inner surface, while no pressure or constraint is applied on the outer surface, as done by [25], and it adopts the method proposed by [26]. The stress distribution equation obtained in this study is different from that proposed by [25] and [26]. Furthermore, this solution has been compared with FEM and experimental results, where the experimental study refers to the research conducted by [27]. From the comparative study, it can be seen that the proposed analytical solution shows good agreement with FEM with an error value of less than 2.77%. In addition, this equation was also validated with experiments. This research has been partially presented at a conference [28], and in this article, it is presented in more detail and comprehensively.

2. Model and Analytical Solution

Figure 1 displays the FGM cylinder model with radial coordinates \bar{r} and displacement coordinates \bar{u} . R_o represents the outermost radius of the cylinder, and its coordinate is defined in Equation (1).

$$r = \bar{r}/R_o , \quad u = \bar{u}/R_o \tag{1}$$

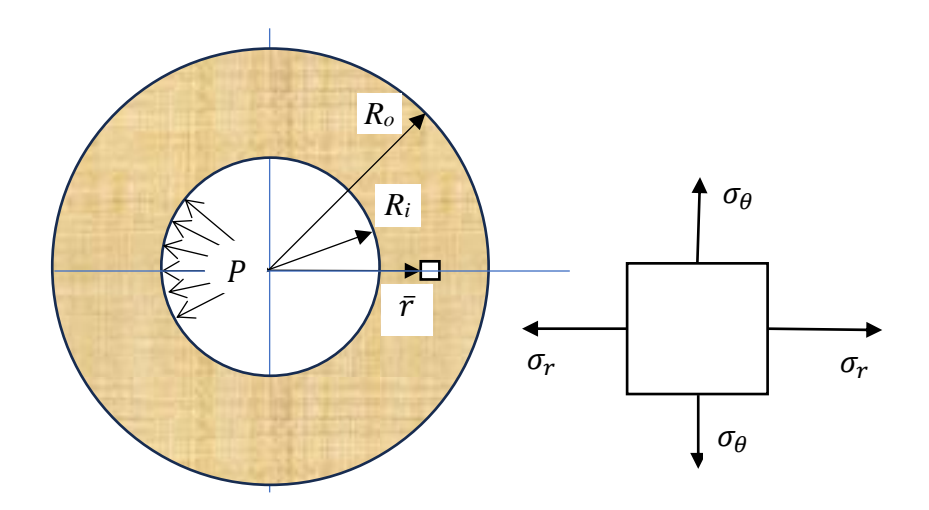


Fig. 1. FGM cylinder cross-section and its coordinate system

Radial strains and hoop strains are analyzed under the plane-strain assumption, so the equilibrium equation is given as shown in Equation (2) [25], [26], [28].

$$\varepsilon_{\theta} = \varepsilon_{\phi} = \frac{u}{r} \quad \varepsilon_{r} = \frac{du}{dr}, \quad \gamma_{r\theta} = \gamma_{r\phi} = \gamma_{\theta\phi} = 0$$
 (2)

The material is assumed to be isotropic, with a constant Poisson's ratio and a radially varying Young's modulus. Using the power function, the value of elasticity in radius variation can be seen in Equation (3) [25]. E_o is the value of Young's modulus on the outermost surface $(r/R_o = 1)$, and β is the gradient constant of inhomogeneity.

$$E(r) = E_0 r^{\beta} \tag{3}$$

The constitutive equation can be seen in Equation (4) and Equation (5).

$$\sigma_r = C_{11}\varepsilon_r + C_{12}\varepsilon_\theta, \quad \sigma_\theta = C_{12}\varepsilon_r + C_{11}\varepsilon_\theta + C_{12}\varepsilon_\phi \tag{4}$$

Here,

$$C_{11} = c_{11}r^{\beta} = \left(\frac{E_o(1-v)}{(1+v)(1-2v)}\right)r^{\beta}, \quad C_{12} = c_{12}r^{\beta} = \left(\frac{E_ov}{(1+v)(1-2v)}\right)r^{\beta}$$
 (5)

The non-trivial equilibrium is Equation (6), and radial displacement is Equation (7).

$$\frac{d\sigma_r}{dr} + \frac{\sigma_r - \sigma_\theta}{r} = 0 \tag{6}$$

$$r^{2}u'' + (\beta + 1)ru' + (v^{*}\beta - 1)u = 0$$
(7)

The symbol v^* is a simplified form of the Poisson's ratio, where $v^* = v/(1-v)$. Equation (7) can be solved using the second-order Cauchy–Euler equation, assuming the solution as shown in Equation (8). The characteristics of the equation and its roots are given in Equations (9) and (10), respectively.

$$u = r^m, \quad \frac{du}{dr} = mr^{m-1}, \quad \frac{d^2u}{dr^2} = m(m-1)r^{m-2}$$
 (8)

$$m^2 + \beta m + (v^*\beta - 1) = 0 \tag{9}$$

$$m_1 = \frac{1}{2} \left(-\beta - \sqrt{\beta^2 - 4(v^*\beta - 1)} \right), \qquad m_2 = \frac{1}{2} \left(-\beta + \sqrt{\beta^2 - 4(v^*\beta - 1)} \right)$$
 (10)

To solve for the variable *m*, there are three conditions based on the Cauchy-Euler formula. These conditions are as follows [26].

• The values m_1 and m_2 are real and different $(m_1 \neq m_2)$; then the solution is as seen in Equation (11).

$$u = Ar^{m_1} + Br^{m_2} \tag{11}$$

• The values m_1 and m_2 are real and equal $(m_1 = m_2 = m)$; then the solution is as seen in Equation (12).

$$u = (A + B \ln r)r^m \tag{12}$$

• The values m_1 and m_2 are imaginary $(m_1 = x + yi, m_2 = x - yi)$; then the solution is as seen in Equation (13).

$$u = (A\cos(y\ln r) + B\sin(y\ln r))r^{x}$$
(13)

Since the material has a Poison value ratio of 0 < v < 0.5, then $0 < v^* < 1$, and $0 < v^{*2} < 1$. Thus, the value of the square under the root sign in equation (10) is as seen in Equation (14).

$$\Delta = \beta^2 - 4(v^*\beta - 1) = (\beta^2 - 2v^*)^2 + 4(1 - v^{*2}) > 0$$
(14)

The values *A* and *B* are parameters that depend on two boundary conditions [25]:

- (1) Boundary condition 1: On the inner surface of the cylinder, internal pressure, *P*, is applied as seen in Equation (15).
- (2) Boundary condition 2: On the outer surface of the cylinder, no pressure is applied, as seen in Equation (16).

Boundary condition 1:
$$\sigma_r \left(\frac{R_i}{R_o}\right) = -P$$

$$\varepsilon_r = m_1 A \left(\frac{R_i}{R_o}\right)^{m_2 - 1} + m_2 B \left(\frac{R_i}{R_o}\right)^{m_2 - 1}; \quad \varepsilon_\theta = A \left(\frac{R_i}{R_o}\right)^{m_1 - 1} + B \left(\frac{R_i}{R_o}\right)^{m_2 - 1}$$
(15)

Boundary condition 2:
$$\sigma_r \left(\frac{R_o}{R_o} \right) = 0$$

$$\varepsilon_r = m_1 A + m_2 B; \qquad \varepsilon_\theta = A + B$$
(16)

Parameter *A* and parameter *B* can be obtained in the following stages:

• Determine parameter *B* by eliminating parameter *A* from boundary condition 1 and boundary condition 2.

From boundary condition 1: Substitute Equation (4) into Equation (15) as seen in Equation (17).

$$-P = C_{11}\varepsilon_{r} + C_{12}\varepsilon_{\theta}$$

$$-P = \left(\frac{E_{o}(1-v)}{(1+v)(1-2v)}\right) \left(\frac{R_{i}}{R_{o}}\right)^{\beta} \left(m_{1}A\left(\frac{R_{i}}{R_{o}}\right)^{m_{1}-1} + m_{2}B\left(\frac{R_{i}}{R_{o}}\right)^{m_{2}-1}\right)$$

$$+ \left(\frac{E_{o}v}{(1+v)(1-2v)}\right) \left(\frac{R_{i}}{R_{o}}\right)^{\beta} \left(A\left(\frac{R_{i}}{R_{o}}\right)^{m_{1}-1} + B\left(\frac{R_{i}}{R_{o}}\right)^{m_{2}-1}\right)$$
(17)

Suppose:

$$X = \left(\frac{E_0(1-v)}{(1+v)(1-2v)}\right), \text{ and } Y = \left(\frac{E_0v}{(1+v)(1-2v)}\right)$$
 (18)

Arrange Equation (17) into Equation (19).

$$-P = X \left(\frac{R_{i}}{R_{o}}\right)^{\beta} m_{1} A \left(\frac{R_{i}}{R_{o}}\right)^{m_{1}-1} + X \left(\frac{R_{i}}{R_{o}}\right)^{\beta} m_{2} B \left(\frac{R_{i}}{R_{o}}\right)^{m_{2}-1} + Y \left(\frac{R_{i}}{R_{o}}\right)^{\beta} A \left(\frac{R_{i}}{R_{o}}\right)^{m_{1}-1} + Y \left(\frac{R_{i}}{R_{o}}\right)^{\beta} B \left(\frac{R_{i}}{R_{o}}\right)^{m_{2}-1} = \left(X \left(\frac{R_{i}}{R_{o}}\right)^{\beta} m_{1} \left(\frac{R_{i}}{R_{o}}\right)^{m_{1}-1} + Y \left(\frac{R_{i}}{R_{o}}\right)^{\beta} \left(\frac{R_{i}}{R_{o}}\right)^{m_{1}-1}\right) A + \left(X \left(\frac{R_{i}}{R_{o}}\right)^{\beta} m_{2} \left(\frac{R_{i}}{R_{o}}\right)^{m_{2}-1} + Y \left(\frac{R_{i}}{R_{o}}\right)^{\beta} \left(\frac{R_{i}}{R_{o}}\right)^{m_{2}-1}\right) B$$

$$(19)$$

Parameter A can be obtained as seen in Equation (20).

$$-A = \frac{P\left(\frac{R_i}{R_o}\right)^{1-\beta} (1+v)(1-2v) + (E_o(1-v)m_2 + E_o v) \left(\frac{R_i}{R_o}\right)^{m_2} B}{(E_o(1-v)m_1 + E_o v) \left(\frac{R_i}{R_o}\right)^{m_1}}$$
(20)

From the boundary condition 2: Substitute Equation (4) into Equation (16) as seen in Equation (21).

$$0 = C_{11}\varepsilon_r + C_{12}\varepsilon_\theta \tag{21}$$

We obtain Equation (22) by assuming *X* and *Y* as written in Equation (18).

$$0 = Xm_1A + Xm_2B + YA + YB = (Xm_1 + Y)A + (Xm_2 + Y)B$$
 (22)

Parameter A can be obtained as seen in Equation (23).

$$A = \frac{-B(E_o(1-v)m_2 + E_o v) \left(\frac{R_i}{R_o}\right)^{m_1}}{(E_o(1-v)m_1 + E_o v) \left(\frac{R_i}{R_o}\right)^{m_1}}$$
(23)

Parameter B can be obtained by eliminating parameter A by adding Equation (20) and Equation (23), as seen in Equation (24).

$$B = \frac{P\left(\frac{R_i}{R_O}\right)^{1-\beta} (1+\nu)(1-2\nu)}{E_O\left(\left(\frac{R_i}{R_O}\right)^{m_1} - \left(\frac{R_i}{R_O}\right)^{m_2}\right)(\nu + (1-\nu)m_2)}$$
(24)

• Determine parameter *A* by eliminating parameter *B* from boundary condition 1 and boundary condition 2.

Similar to point (1), from boundary condition 1 and boundary condition 2, parameter B is obtained as seen in Equation (25) and Equation (26), respectively.

$$-B = \frac{P\left(\frac{R_i}{R_o}\right)^{1-\beta} (1+v)(1-2v) + (E_o(1-v)m_1 + E_ov)\left(\frac{R_i}{R_o}\right)^{m_1} A}{(E_o(1-v)m_2 + E_ov)\left(\frac{R_i}{R_o}\right)^{m_2}}$$
(25)

$$B = \frac{-A(E_o(1-v)m_1 + E_ov)\left(\frac{R_i}{R_o}\right)^{m_2}}{(E_o(1-v)m_2 + E_ov)\left(\frac{R_i}{R_o}\right)^{m_2}}$$
(26)

Parameter A is obtained by eliminating parameter B by adding Equation (25) and Equation (26), as seen in Equation (27).

$$A = -\frac{P\left(\frac{R_i}{R_O}\right)^{1-\beta} (1+\nu)(1-2\nu)}{E_O\left(\left(\frac{R_i}{R_O}\right)^{m_1} - \left(\frac{R_i}{R_O}\right)^{m_2}\right)(\nu + (1-\nu)m_1)}$$
(27)

From Equation (4), radial stress can be determined as shown in Equation (28). By substituting parameter A as defined in Equation (27) and parameter B as defined in Equation (24), the radial stress is obtained as shown in Equation (29).

ss is obtained as shown in Equation (29).
$$\sigma_{r} = C_{11}\varepsilon_{r} + C_{12}\varepsilon_{\theta},$$

$$= \left(\frac{E_{0}(1-v)}{(1+v)(1-2v)}\right)r^{\beta}(m_{1}Ar^{m_{1}-1} + m_{2}Br^{m_{2}-1}) + \left(\frac{E_{0}v}{(1+v)(1-2v)}\right)r^{\beta}(Ar^{m_{1}-1} + Br^{m_{2}-1})$$
(28)
$$Br^{m_{2}-1})$$

$$\sigma_r = \frac{P\left(\frac{R_i}{R_o}\right)^{1-\beta} (r^{m_1} - r^{m_2})r^{\beta - 1}}{\left(\frac{R_i}{R_o}\right)^{m_1} - \left(\frac{R_i}{R_o}\right)^{m_2}}$$
(29)

Similarly, from Equation (4), hoop stress can be determined as seen in Equation (30). By substituting parameter A as written in Equation (27) and parameter B as written in Equation (24), the hoop stress is obtained as seen in Equation (31). The simple form is as written in Equation (32), where χ_1 and χ_2 are as stated by Equation (33).

$$\sigma_{\theta} = C_{12}\varepsilon_{r} + C_{11}\varepsilon_{\theta}$$

$$= \left(\frac{E_{o}v}{(1+v)(1-2v)}\right)r^{\beta}(m_{1}Ar^{m_{1}-1} + m_{2}Br^{m_{2}-1})$$

$$+ \left(\frac{E_{o}(1-v)}{(1+v)(1-2v)}\right)r^{\beta}(Ar^{m_{1}-1} + Br^{m_{2}-1})$$
(30)

 $= \frac{Pr^{m_1}(vm_1 + (1-v))(m_2(v-1) - 1)\left(\frac{R_i}{R_o}\right)^{1-\beta}r^{\beta-1} - Pr^{m_2}(vm_2 + (1-v))(m_1(v-1) - 1)\left(\frac{R_i}{R_o}\right)^{1-\beta}r^{\beta-1}}{(m_1(v-1) - 1)(m_2(v-1) - 1)\left(\left(\frac{R_i}{R_o}\right)^{m_1} - \left(\frac{R_i}{R_o}\right)^{m_2}\right)}$ (31)

$$\sigma_{\theta} = \frac{\left(\frac{R_{i}}{R_{o}}\right)^{1-\beta} r^{\beta-1} (\chi_{1} - \chi_{2})}{(m_{1}(v-1) - v)(m_{2}(v-1) - v)\left(\left(\frac{R_{i}}{R_{o}}\right)^{m_{1}} - \left(\frac{R_{i}}{R_{o}}\right)^{m_{2}}\right)}$$
(32)

$$\chi_1 = Pr^{m_2} (vm_2 + (1-v))(m_1(v-1) - v)
\chi_2 = Pr^{m_1} (vm_1 + (1-v))(m_2(v-1) - v)$$
(33)

3. Results and Discussion

The analytical solution proposed in the present study will be validated by comparing FEM and experimental analysis. In the FEM analysis, the cylinder is assumed to be an axisymmetric plane stress by creating layers of material with different stiffness, as has been done in a previous study [28]. Each layer has a thickness value of $(0.6 < r/R_o < 1)$ which refers to previous research [25].

The radial and hoop stress distributions are shown for each general inhomogeneity constant (-2 < β < 2). Meanwhile, the validation of the present study against experimental studies is by comparing it with previous research [27], which performed experiments on thick-walled cylinders by applying internal pressure caused by the penetration of a tapered cylinder.

3.1. FEM Validation

The finite element model developed in this study refers to the work of Gashemi [29], as presented in Table 1. The simulation employs the PLANE183 element type, with material properties defined by Young's modulus (E) and Poisson's ratio (ν). Incorporates a quadrilateral mesh configuration with axisymmetric behavior and internal pressure in the FEM model was applied as a surface load. Figure 2 presents the model along with the corresponding meshing results.

Table 1. Model and parameters [29].

Parameters	Symbol	Value	Unit
Internal Pressure	Р	7	MPa
Inner Radius	R_i	30	mm
Outer Radius	R_o	50	mm
Inhomogeneity Constanta	$oldsymbol{eta}$	-2, -1, 0, 1, 2	-
Poisson's Ratio	ν	0.3	-
Young's Modulus	E	72	GPa

Convergence tests have been conducted to evaluate the effect of the number of cylindrical layers on the stability of the stress values, as shown in Figure 3. The results indicate that convergence begins at a layer count of n = 20, but a more precise data stability occurs at n = 160. A comparison of the stress values from FEM in this study against reference studies can be seen in Table 2, with a maximum error rate of 4.32% for hoop stress. These results indicate that the accuracy of the FEM method in this study can be considered sufficient.

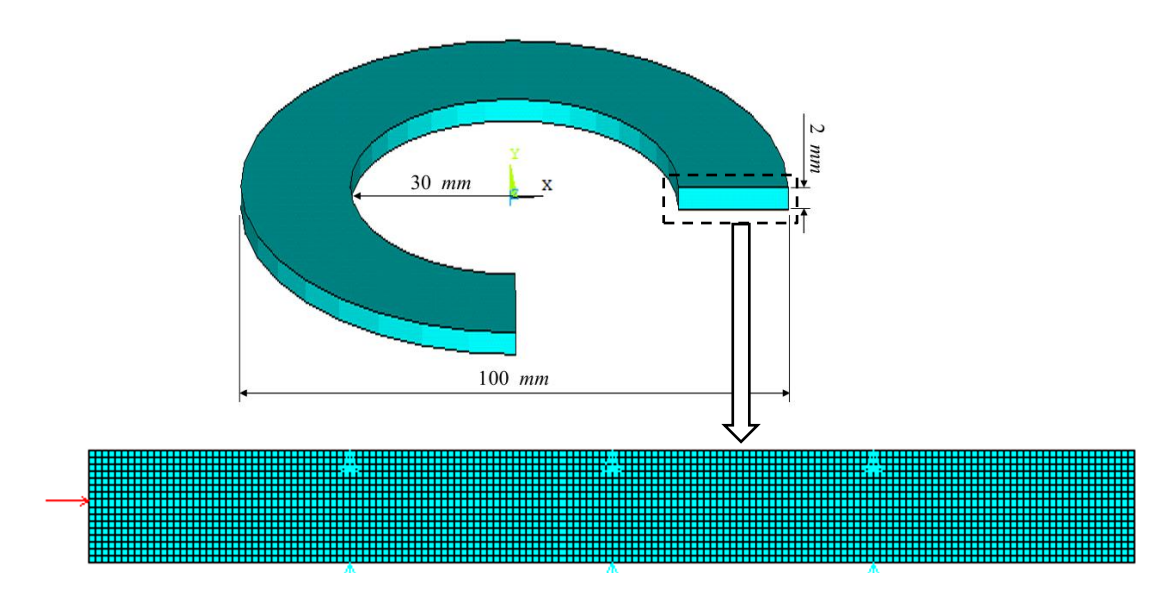


Fig. 2. The model, along with the corresponding meshing results

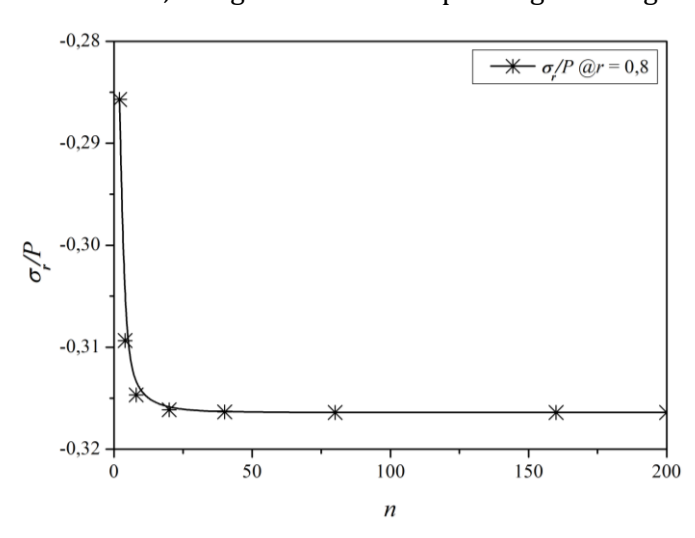


Fig. 3. Convergence Behavior of Stress Values to the Number of Cylinder Layers (n)

The next step is to validate the analytical solution developed in the present study against the FEM simulation results. The important themes discussed are radial and hoop stress distribution for general inhomogeneity constants. For radial stress, the solution previously proposed by [25] is the

same as the solution in the present study, as seen in Figures 4(a) and 4(b). Both solutions are valid when compared to FEM analysis; thus, there are no issues with these solutions and they are not important to discuss further. However, the problem is that the hoop stress distribution solution proposed by [25] is invalid when compared to the FEM analysis, as seen in Figure 5(a). For this reason, a new solution is proposed in the present study and proven to be valid for all inhomogeneity constants $(-2 < \beta < 2)$, as can be seen in Figure 5(b).

T 1.1. 2 A	. (1)		v against reference studies.
I ania / // comparicon	At the ctreec value tr	om beivein thic ctild	U AGAINET PAFAPANCA EFIIGIAE
I aute 4. A cultival ison	OF THE STRESS VALUES II	OIII I LIVI III UIIS SUUU	v agamst reference studies.

r/R_0 Present S		t Study	tudy Ghasemi[2		Erro	or (%)	
17K0	σ_r/P	$\sigma_{ heta}/P$	σ_r/P	σ_{θ}/P	σ_r/P	σ_{θ}/P	
0.60	-0.9971	1.6757	-1.0000	1.6160	0.2857	3.6952	
0.65	-0.8000	1.6243	-0.8020	1.5570	0.2494	4.3215	
0.70	-0.6343	1.5857	-0.6350	1.5250	0.1125	3.9813	
0.75	-0.4914	1.5571	-0.4910	1.5020	0.0873	3.6713	
0.80	-0.3671	1.5357	-0.3670	1.4860	0.0389	3.3455	
0.85	-0.2586	1.5200	-0.2590	1.4740	0.1655	3.1208	
0.90	-0.1629	1.5100	-0.1630	1.4670	0.0876	2.9312	
0.95	-0.0771	1.5029	-0.0770	1.4630	0.1855	2.7243	
1.00	0.0000	1.4257	0.0000	1.4540	0.0000	1.9500	

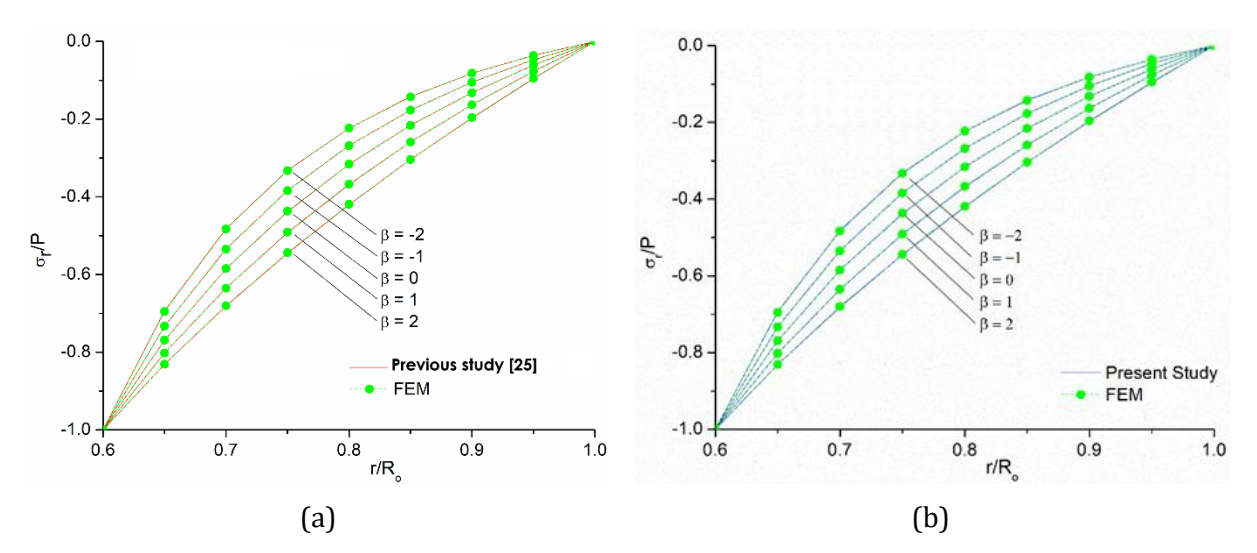


Fig. 4. Validation of radial stress to FEM (a) Previous study [25], (b) Present study

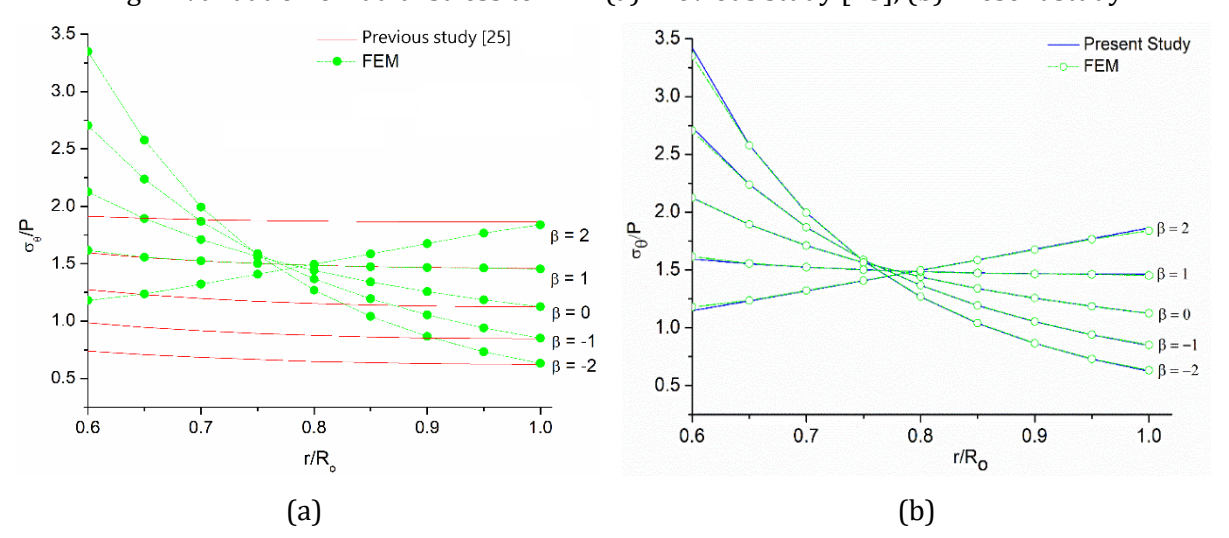


Fig. 5. Validation of hoop stress to FEM (a) Previous study [25], (b) Present study

Several noteworthy observations indicate that stress distribution can be effectively controlled through engineered material gradation using FGMs [30]; in particular, for hoop stress in FGM cylinders, a more uniform hoop stress distribution can be achieved, especially when the value of β equals 1 [31]. A recent numerical investigation by [32] also demonstrated that variations in the inhomogeneity parameter and Poisson's ratio significantly influence the thermoelastic stress and displacement fields in rotating thick-walled FGM cylinders, reinforcing the importance of accurate modeling in pressure vessel design under coupled mechanical and thermal loads

3.2. Experimental Validation

Experimental validation refers to previous research [27], with equipment as seen in Figure 6. Radial and hoop stresses are measured at several points on a cylinder made of homogeneous material (inhomogeneity constant β = 0). The penetration of a tapered cylinder results in pressure on the inner surface of the cylinder, which is considered to represent internal pressure. Several strain gauges were installed at the appropriate points and orientations to measure the radial and hoop strain within the range of R_i = 90.5 mm to R_o = 140.5 mm.

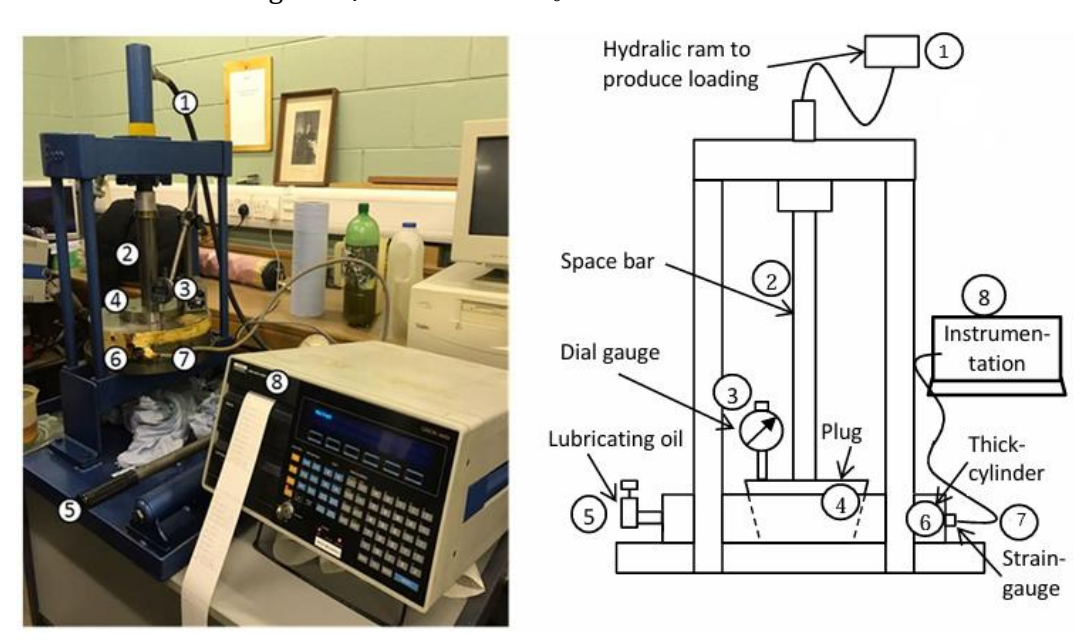


Fig. 6 Equipment used for the experiment and a schematic drawing showing all the parts of the apparatus and their interconnections [27]

Table 3. The strain	gauge readings f	for variations in p	penetration depth

Penetration depth (mm)	0.96	1.92	2.64	3.26	4.48
Channel no.		Strain g	gauge reading	gs	
1	-11	-30	-44	-55	-80
3	-16	-41	-61	-77	-111
5	-25	-55	-79	-99	-144
7	-30	-78	-117	-151	-220
9	-37	-110	-200	-264	-334
11	53	110	155	198	271
13	61	128	180	227	312
15	69	149	210	265	366
17	77	178	251	317	439
19	94	222	313	398	551

Table 3 shows the strain gauge readings for variations in penetration depth. In the experiment, channels 1, 3, 5, 7, and 9 are strain gauges used to measure radial stress, while channels 11, 13, 15, 17, and 19 are strain gauges used to measure hoop stress. For ease of understanding, the data in

Table 3 is rearranged to show the radial strain and hoop strain values at variations in radius values, respectively, as shown in Table 4.

Table 4. The radial strain and hoop strain values at variations in radius values

n (mm)	Tymes of strain sauges	Strain gauge readings on each space bar penetration (μm)					
r (mm)	Types of strain gauges	0.96 mm	1.92 mm	2.64 mm	3.26 mm	4.48 mm	
90.5	$arepsilon_r$	-37	-110	-200	-264	-334	
90.3	$arepsilon_{ heta}$	94	222	313	398	551	
1020	$arepsilon_r$	-30	-78	-117	-151	-220	
103.0	$arepsilon_{ heta}$	77	178	251	317	439	
115.5	$arepsilon_r$	-25	-55	-79	-99	-144	
115.5	$arepsilon_{ heta}$	69	149	210	265	366	
128.0	$arepsilon_r$	-16	-41	-61	-77	-111	
	$arepsilon_{ heta}$	61	128	180	227	312	
140.5	$arepsilon_r$	-11	-30	-44	-55	-80	
	$arepsilon_{ heta}$	53	110	155	198	271	

Radial stress is calculated by Equation (34), and hoop stress is calculated by Equation (35). Table 5 shows radial and hoop stress variations at radius (r) values.

$$\sigma_r = \frac{E}{1 - v^2} (\varepsilon_r + v\varepsilon_\theta) \tag{34}$$

$$\sigma_{\theta} = \frac{E}{1 - v^2} (\varepsilon_{\theta} + v \varepsilon_r) \tag{35}$$

Table 5. Radial and hoop stress at radius (*r*) values variations

()	Stress	Stress value on each space bar penetration (MPa)					
<i>r</i> (mm)	orientation	0.96 mm	1.92 mm	2.64 mm	3.26 mm	4.48 mm	
90.5	σ_r	-2.011	-9.920	-24.251	-33.051	-38.560	
90.5	$\sigma_{ heta}$	18.949	43.200	57.829	72.869	103.040	
103	σ_r	-1.577	-5.623	-9.531	-12.777	-20.183	
103	$\sigma_{ heta}$	15.543	35.337	49.349	62.103	85.257	
115.5	σ_r	-0.983	-2.354	-3.657	-4.457	-7.817	
	$\sigma_{ heta}$	14.057	30.286	42.583	53.783	73.783	
128	σ_r	0.526	-0.594	-1.600	-2.034	-3.977	
	$\sigma_{ heta}$	12.846	26.446	36.960	46.606	63.703	
140.5	σ_r	1.120	0.686	0.571	1.006	0.297	
	$\sigma_{ heta}$	11.360	23.086	32.411	41.486	56.457	

Table 6. The equivalent internal pressures

Space bar penetration (mm)	Internal Pressure (MPa)
0.96	3.13
1.92	15.15
2.64	40.05
3.26	55.40
4.48	61.65

The next step is to convert the depth of penetration of the space bar into internal pressure, assuming that the radial stress on the inner surface is equal to the internal pressure. The equivalence between the penetration depth of the space bar and the internal pressure is obtained from the regression process and is assumed to be a 2nd-order polynomial, as shown in Table 6.

Thus, the radial stress and hoop stress distribution graphs can be plotted with equivalent internal pressure, as shown in Figures 7, 8, 9, 10, and 11.

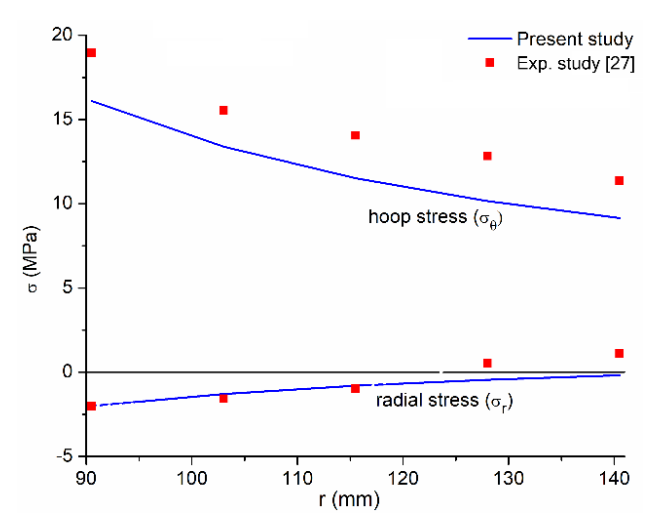


Fig. 7. Radial and hoop stress with a penetration of the space bar of 0.96 mm (P = 3.13 MPa)

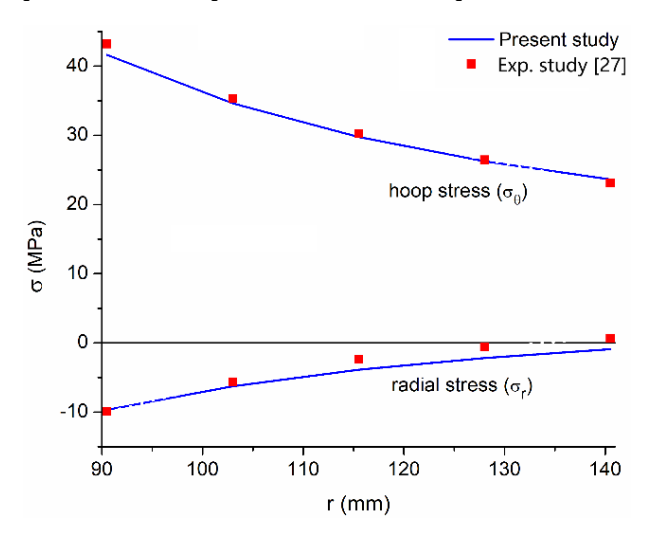


Fig. 8. Radial and hoop stress with a penetration of the space bar of 1.92 mm (P = 15.15 MPa)

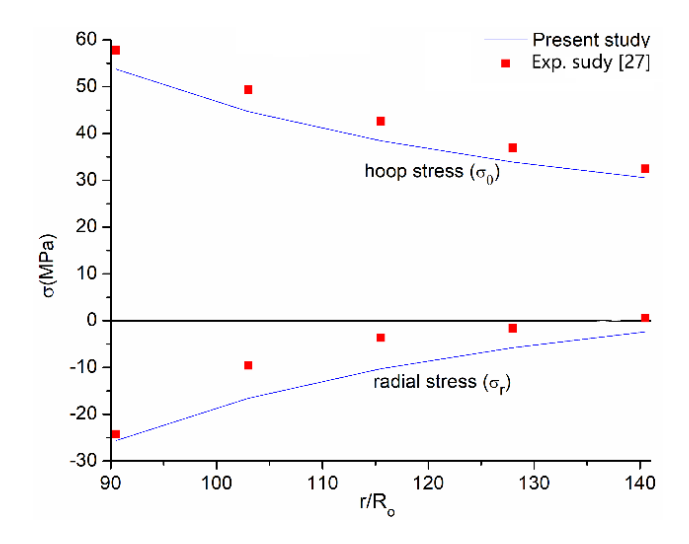


Fig. 9. Radial and hoop stress with a penetration of the space bar of 2.64 mm (P = 40.05 MPa)

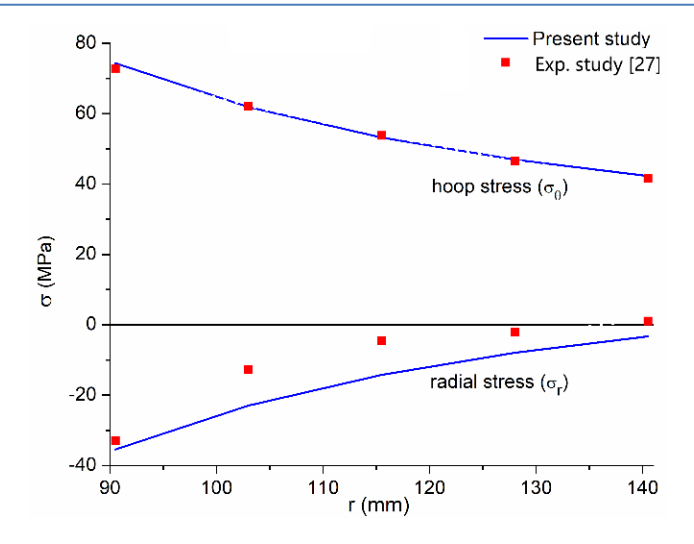


Fig. 10. Radial and hoop stress with a penetration of the space bar of 3.26 mm (P = 55.40 MPa)

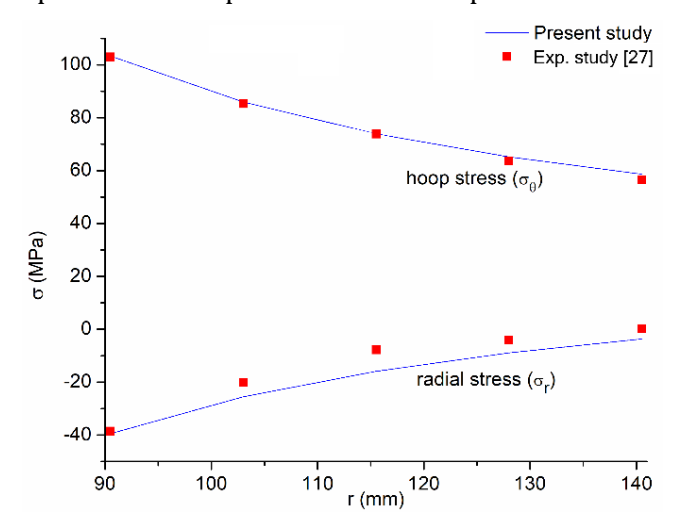


Fig. 11. Radial and hoop stress with a penetration of the space bar of 4.48 mm (P = 61.65 MPa)

The experimental validation conducted in this study has confirmed the reliability of the proposed analytical solution, although only in the homogeneous case (β = 0). For other values of β , further investigation remains to be conducted in the future. Additionally, the feasibility of using the tapered cylindrical penetration technique to simulate internal pressure in thick-walled cylinders has been acknowledged, as also reported by [33]. This approach is particularly valuable when direct pressurization is not practical, either technically or economically. Regression analysis, which links the depth of penetration with the equivalent internal pressure through a second-order polynomial, allows for the practical translation of experimental displacement measurements into stress conditions within the analytical domain. This mapping is crucial for bridging the gap between physical testing and theoretical modeling.

4. Conclusions

The use of functionally graded materials (FGMs) offers a strategic solution to meet the demands of modern industry, owing to their customizable nature that allows for specific property requirements in engineering applications. Previous researchers have proposed analytical solutions for stress distribution in the radial direction, but those solutions are not accurate for general inhomogeneity constants. The present study introduces a more accurate analytical solution to overcome these limitations. In this formulation, the characteristics of material inhomogeneity are defined using a power function, and internal pressure is applied under axisymmetric conditions.

The analytical solution in this present study has been validated with the finite element method (FEM) model, with a maximum error of less than 2.77%. The FEM model was created with sizes

and parameters referring to previous similar studies. The type of element used is PLANE183, defining material properties based on elastic modulus and Poisson's ratio. The model is divided into 160 layers based on convergence testing. The FEM results obtained have been consistent and valid compared to previous reference comparisons and are considered suitable for use. Furthermore, the validation of the experimental study also shows the accuracy of the proposed analytical solution, although it is limited only to homogeneous materials with an inhomogeneity constant β equal to zero. It is important to acknowledge that experimental validation for materials with non-zero β values has not been conducted, and further research is needed for the future.

The main contribution of this research lies in the specific boundary conditions: internal pressure is applied to the inner surface while the outer surface remains pressure-free. Caution should be emphasized when extending the application beyond these conditions. To strengthen the analysis, several previous studies involving FGM under various loading conditions have been reviewed to highlight the novelty and relevance of this work in advancing the analytical approach for graded materials. The proposed solution provides a reliable and practical framework for the design and evaluation of FGM cylinders, particularly in high-pressure applications where material gradation has a significant impact on structural behavior. Future research is expected to extend the experimental validation to a wider range of β values and investigate more complex boundary conditions, thus improving the general applicability of the developed analytical model.

Acknowledgement

The authors would like to acknowledge the support provided by Universitas Lampung through the Professorship Grant 2024, under Contract No. 539/UN26.21/PN/2024, dated April 24, 2024.

LIST	01	NO	tati	ons

Symbol	Description	Unit
r	Radial coordinate	-
R_i	Inner radius of the cylinder	mm
R_o	Outer radius of the cylinder	mm
u(r)	Radial displacement as a function of r	-
σ_r	Radial stress	MPa
$\sigma_{ heta}$	Hoop (circumferential) stress	MPa
E(r)	Young's modulus as a function of r	GPa
v	Poisson's ratio (assumed constant)	-
β	Inhomogeneity constant	-
A, B	Constants determined by boundary conditions	-
P	Internal pressure applied to the inner surface	MPa
$arepsilon_r$	Radial strain	-
$arepsilon_{ heta}$	Hoop (circumferential) strain	-

References

- [1] Karamanli A, Vo TP. Size-dependent behaviour of functionally graded sandwich microbeams based on the modified strain gradient theory. Composite Structures. 2020;246:112401. https://doi.org/10.1016/j.compstruct.2020.112401
- [2] Mathew C, Ejiofor O. Mechanics and computational homogenization of effective material properties of functionally graded (composite) material plate FGM. Int J Sci Res Publ. 2023;13(9):128-50. https://doi.org/10.29322/IJSRP.13.09.2023.p14120
- [3] El-Galy IM, Saleh BI, Ahmed MH. Functionally graded materials classifications and development trends from industrial point of view. SN Appl Sci. 2019;1(11):1378. doi:10.1007/s42452-019-1413-4. https://doi.org/10.1007/s42452-019-1413-4
- [4] Wen Z, Li M. Compressive properties of functionally graded bionic bamboo lattice structures fabricated by FDM. Materials. 2021;14(16):4410. https://doi.org/10.3390/ma14164410
- [5] Petit C, Montanaro L, Palmero P. Functionally graded ceramics for biomedical application: Concept, manufacturing, and properties. Int J Appl Ceram Technol. 2018;15(4):820-40. https://doi.org/10.1111/ijac.12878

- [6] Jung W-Y, Han S-C. Transient analysis of FGM and laminated composite structures using a refined 8-node ANS shell element. Compos Part B Eng. 2014;56:372-83. https://doi.org/10.1016/j.compositesb.2013.08.044
- [7] Dose G, Roccella S, Romanelli F. Engineering of a FGM interlayer to reduce the thermal stresses inside the PFCs. Appl Sci. 2022;12(20):10215. https://doi.org/10.3390/app122010215
- [8] Sofiyev AH, Kuruoğlu N. The stability of FGM truncated conical shells under combined axial and external mechanical loads in the framework of the shear deformation theory. Compos Part B Eng. 2016;92:463-76. https://doi.org/10.1016/j.compositesb.2016.02.027
- [9] Chu L, Dui G. Exact solutions for functionally graded micro-cylinders in first gradient elasticity. Int J Mech Sci. 2018;148:366-73. https://doi.org/10.1016/j.ijmecsci.2018.09.011
- [10] Amos SO. Numerical analysis and material selection of functionally graded pipes based on metals and ceramics for deep offshore oil and gas operations in Gulf of Guinea. 2020 [cited 2024 Dec 17].
- [11] Pachaiappan S, Chandrasekaran S. Numerical analysis of offshore topside with FGM under impact loads. Innov Infrastruct Solut. 2022;7(3):195. https://doi.org/10.1007/s41062-022-00802-2
- [12] Wang ZW, Zhang Q, Xia LZ, Wu JT, Liu PQ. Stress analysis and parameter optimization of an FGM pressure vessel subjected to thermo-mechanical loadings. Procedia Eng. 2015;130:374-89. https://doi.org/10.1016/j.proeng.2015.12.230
- [13] Habib E-S, El-Hadek MA, El-Megharbel A. Stress analysis for cylinder made of FGM and subjected to thermo-mechanical loadings. Metals. 2018;9(1):4. https://doi.org/10.3390/met9010004
- [14] Ghannad M, Yaghoobi MP. 2D thermo elastic behavior of a FG cylinder under thermomechanical loads using a first order temperature theory. Int J Press Vessels Pip. 2017;149:75-92. https://doi.org/10.1016/j.ijpvp.2016.12.002
- [15] Lo K-C, Lai H-Y. Corrosion enhancement for FGM coolant pipes subjected to high-temperature and hydrostatic pressure. Coatings. 2022;12(5):666. https://doi.org/10.3390/coatings12050666
- [16] Yaghoobi MP, Ghannad M. An analytical solution for heat conduction of FGM cylinders with varying thickness subjected to non-uniform heat flux using a first-order temperature theory and perturbation technique. Int Commun Heat Mass Transf. 2020;116:104684. https://doi.org/10.1016/j.icheatmasstransfer.2020.104684
- [17] Doan TN, Nguyen AT, Van Binh P, Van Hung T, Tru VQ, Luat DT. Static analysis of FGM cylindrical shells and the effect of stress concentration using quasi-3D type higher-order shear deformation theory. Composite Structures. 2021;262:113357. https://doi.org/10.1016/j.compstruct.2020.113357
- [18] Shiyekar SM, Awari A. Static stress analysis of functionally graded cylindrical stiffened shells. ASPS Conf Proc. 2022;1(1):1847-52. https://doi.org/10.38208/acp.v1.727
- [19] Sofiyev AH, Hui D. On the vibration and stability of FGM cylindrical shells under external pressures with mixed boundary conditions by using FOSDT. Thin-Walled Struct. 2019;134:419-27. https://doi.org/10.1016/j.tws.2018.10.018
- [20] Han Y, Zhu X, Li T, Yu Y, Hu X. Free vibration and elastic critical load of functionally graded material thin cylindrical shells under internal pressure. Int J Struct Stab Dyn. 2018;18(11):1850138. https://doi.org/10.1142/S0219455418501389
- [21] Gao G, Sun N, Shao D, Tao Y, Zhang H. Nonstationary response system for the stepped composite cylindrical shell with drop-off ply under moving random loads. Ocean Eng. 2024;298:117178. https://doi.org/10.1016/j.oceaneng.2024.117178
- [22] Chen X, Drost L, Peters DJ. Hydrodynamic response of submerged floating tunnel in combined wave-current flows. In: Sapountzakis EJ, Banerjee M, Biswas P, Inan E, editors. Proc 14th Int Conf Vib Probl. Lecture Notes Mech Eng. Singapore: Springer; 2021. p. 807-22. https://doi.org/10.1007/978-981-15-8049-9_49
- [23] Lin F, et al. Damage characteristics and dynamic response of RC shells subjected to underwater shock wave. Appl Sci. 2024;14(5):1878. https://doi.org/10.3390/app14051878
- [24] Nugraha N, Akmal J, Lubis A. Submerged floating tunnel bridge (SFTB): A status report and evaluation of technology readiness level (TRL). J Integr Adv Eng. 2022;2(1):19-32. https://doi.org/10.51662/jiae.v2i1.35
- [25] Tutuncu N, Ozturk M. Exact solutions for stresses in functionally graded pressure vessels. Compos Part B Eng. 2001;32(8):683-6. https://doi.org/10.1016/S1359-8368(01)00041-5
- [26] Xie J, Hao S, Wang W, Shi P. Analytical solution of stress in functionally graded cylindrical/spherical pressure vessel. Arch Appl Mech. 2021;91(7):3341-63. https://doi.org/10.1007/s00419-021-01970-w
- [27] Caela JG. Stress distribution in a tick cylinder. 2017 [cited 2024 Dec 17].
- [28] Murti AW, Akmal J, Lubis A, Savetlana S. Exact and numerical solution for stress analysis on FGM cylindrical shell using axisymmetric element with plane stress. In: AIP Conf Proc. AIP Publishing; 2023. https://doi.org/10.1063/5.0115295
- [29] Ghasemi AR, Kazemian A, Moradi M. Analytical and numerical investigation of FGM pressure vessel reinforced by laminated composite materials. 2014.

- [30] Chitour M, Khadraoui F, Mansouri K, Rebai B, Menasria A, Zemmouri A, Touati S, Boumediri H. A novel high order theory for static bending of functionally graded (FG) beams subjected to various mechanical loads. Res. Eng. Struct. Mater., 2024; 10(4): 1523-1539. http://dx.doi.org/10.17515/resm2024.141me0104rs
- [31] Sahu RK, Sondhi L, Bhowmick S, Madan R. Deformation and stress analysis of rotating functionally graded hollow cylindrical body for variable heat generation. Res. Eng. Struct. Mater., 2023; 9(2): 597-616. http://dx.doi.org/10.17515/resm2022.470me0713
- [32] Das P, Benslimane A, Islam MA, Siddiquei AA, Rahman MM, Adil MM. Finite element analysis of a generalized rotating FGM vessel subjected to thermo-mechanical loadings: Effect of Poisson ratio and inhomogeneity parameters. Heliyon. 2024;10(11):e31833. https://doi.org/10.1016/j.heliyon.2024.e31833
- [33] Amodu OA, Adamu AA, Anikoh GA. Investigation on the stress distributions in a thick-walled cylinder with internal pressure. 2025 [cited 2025 May 21].